molecules contains one more non-hydrogen atom than the original chemical formula shows.

References

FAN HAI-FU (1975). *Acta Phys. Sin.* **24**, 57-60.
FAN HAI-FU (1986). *Rigaku J.* **3**(1), 25-30.
FAN HAI-FU, HE LUO, QIAN JIN-ZI & LIU SHI-XIANG (1978). *Acta Phys. Sin.* **27**, 554-558.
FAN HAI-FU, YAO JIA-XING, MAIN, P. & WOOLFSON, M. M. (1983). *Acta Cryst.* A**39**, 566-569.
FAN HAI-FU, YAO JIA-XING & QIAN JIN-ZI (1988). *Acta Cryst.* A**44**, 688-691.
HE CUN-HENG (1987). Unpublished data.
ITO, T. (1973). *Z. Kristallogr.* **137**, 399-411.
ITO, T. & NOWACKI, W. (1974). *Z. Kristallogr.* **139**, 85-102.
LETCHER, R. M., FAN HAI-FU, KE HENG-MING & MAK, T. C. W. (1987). *J. Chem. Res.* (*S*), pp. 60-61.
QIAN JIN-ZI, FU PING-QIU, KONG YOU-HUA & GONG GUO-HONG (1982). *Acta Phys. Sin.* **31**, 577-584.

Acta Cryst. (1990). A**46**, 103-112

Simulation and Application of the Distorted ZOLZ Patterns from Dislocations in Si*

BY G. LU†

Laboratory of Atomic Imaging of Solids, Institute of Metal Research, Chinese Academy of Sciences, Shenyang 110015, *China, and Beijing Laboratory of Electron Microscopy, Chinese Academy of Sciences, Beijing* 100080, *China*

AND J. G. WEN, W. ZHANG‡ AND R. WANG

Department of Physics, Wuhan University, Wuhan 430072, *China*

(*Received* 13 *July* 1989; *accepted* 5 *September* 1989)

Abstract

The previously reported distorted zeroth-order fringes in a bright-field Tanaka pattern from a dislocated region in silicon have been computer simulated and the experimental and the many-beam calculated patterns agree well. Calculations are carried out for nine distinct cases of edge, screw and 60° dislocations in a silicon crystal. The general usefulness of the distortion of the ZOLZ pattern in determining geometrical properties of a dislocation is discussed.

1. Introduction

Carpenter & Spence (1982) reported splitting of higher-order Laue-zone (HOLZ) lines and distortion of the zeroth-order Laue-zone (ZOLZ) pattern in a convergent-beam electron diffraction (CBED) pattern from a dislocation in silicon. They also simulated the splitting of HOLZ lines by a method involving the column approximation and used the splitting of HOLZ lines to determine the Burgers vector of a dislocation. Cherns & Preston (1986) proposed a method to determine the Burgers vector of a dislocation using the splitting of a diffraction line in a defocused CBED pattern. Later, Cherns, Kiely & Preston (1988) used the sense of the displacement of the diffraction peak to deduce the sign of the Burgers vector of the dislocation and this was confirmed by kinematical calculation. Tanaka, Terauchi & Kaneyama (1988) made detailed and extensive calculations to show the influence of various dislocations on the distortion of a diffraction line crossed by a dislocation line, on the basis of isotropic elasticity. They showed that at the crossing region the line of diffraction twists and splits into $n+1$ lines, where $n=\mathbf{g}\cdot\mathbf{b}$. The sense of the shift depends on the sign of n. They also considered the effect of the $\mathbf{g}\cdot\mathbf{b}\times\mathbf{u}$ term when $n=0$ and demonstrated the determination of the Burgers vector of a dislocation in various cases. On the other hand, Bian (1986) reported observation of the relative shift of fringes in a bright-field ZOLZ pattern from a dislocation in Al, where, however, the Burgers vector and line direction of the dislocation ($\mathbf{b}$ and $\mathbf{u}$) were unclear. In a systematic study of the influence of dislocations on the ZOLZ of a CBED pattern, Wen, Wang & Lu (1989) observed a similar shift of ZOLZ fringes in large-angle convergent-beam electron diffraction (LACBED; see Tanaka, Saito, Ueno & Harada, 1980) patterns near a dislocation, as well as compression and elongation of the patterns. They pointed out that this distortion of ZOLZ patterns resulted from the relative movement of two parts of the pattern separated by the shadow image of the dislocation in the direction of the Burgers vector. This

* Project supported by the National Natural Science Foundation of China.

† Also with Physics Department, Wuhan University.

‡ Present address: Department of Mathematics and Physics, Wuhan University of Technology, Wuhan 430070, China.

0108-7673/90/020103-10$03.00

relative movement causes the ZOLZ pattern to be elongated or compressed, or to be out of register, depending upon the relative orientation of **b**, **u** and the position of the incident-beam cross over relative to the specimen. These authors also proposed that this phenomenon could be used to determine the Burgers vector of a dislocation and its sign. To understand the experimental observation and to obtain further insight on the influence of dislocations on the ZOLZ pattern, a proper computer simulation is desired. For this purpose, a computer program is developed based on anisotropic elasticity and dynamical diffraction theory, involving the column approximation, to simulate the LACBED (Tanaka) pattern from a dislocated area. On the other hand, it is sometimes important to make quick *in situ* identification of dislocation geometries during studies of dislocation behavior under the transmission electron microscope. The distorted ZOLZ pattern can be used for this purpose to determine dislocation characters and the sign of the Burgers vector.

In this paper we describe briefly the program (§ 2), and show the calculated Tanaka pattern from possible pure edge, pure screw and 60° dislocations (§ 3). In § 4, application of this distorted ZOLZ pattern in the identification of dislocation is considered, and the advantages and disadvantages of this method discussed. Some conclusions are drawn in § 5.

2. Outline of the program

The wave amplitude, φ_g, at the bottom surface of a specimen containing a dislocation can be given in matrix form (*e.g.* Hirsch, Howie, Nicholson, Pashley & Whelan, 1977) as

$$\mathrm{d}\varphi_g/\mathrm{d}z = \sum_h M_{gh}\varphi_h \qquad (1)$$

where the matrix elements are

$$M_{gh} = \pi(-1/\xi'_{g-h} + i/\xi_{g-h}) \qquad g \neq h$$

$$M_{gg} = \pi[-1/\xi'_0 + 2is_g + 2i\mathrm{d}(\mathbf{g}\,.\,\mathbf{R})/\mathrm{d}z]$$

with z the variable along incident-beam direction, s_g the deviation parameter for beam **g**, **R** the displacement due to a dislocation, ξ_g the extinction distance, ξ'_0 and ξ'_g the mean and the anomalous absorption distances respectively. The displacement field, **R**, is evaluated using Stroh's (1958) formulation and the corresponding Fortran routines of Head, Humble, Clarebrough, Morton & Forwood (1973). The integrating routines written by these authors are also used in the present program with some extension to account for the many-beam situation.

To obtain the amplitude distribution in a zone-axis CBED pattern, one needs to integrate (1) along each incident-beam direction. The incident electrons travel in a cone outside the specimen with its vertex (the beam cross over) above or below the specimen (Fig. 1). Inside the specimen the beam is thought to travel along the zone axis since this direction is that of the vector of energy flow (the Poynting vector, *e.g.* Cowley, 1981) in the symmetrical case, which is the case to which this program is to be applied. The variation of φ_g with the incident-beam direction, **B**, is seen through s_g, which depends on the direction of **B**, and **R**, which varies with the position of the beam path relative to the dislocation. The dependence of the intensity on s_g gives rise to the normal CBED pattern and the variation of the intensity with the beam position relative to the dislocation is responsible for the shadow image in a LACBED pattern. The defocus value DF which defines the level of the beam cross over is an important parameter in the calculation. For a certain s_g range, when DF is close to zero, that is, the beam is focused on the specimen by the condenser lens, the calculated intensity distribution corresponds to a normal CBED pattern. If DF is large, either positive or negative (*i.e.* below or above the specimen), we will have a portion of a LACBED pattern (the Tanaka pattern).

Fig. 2 is the program flow chart. After reading in data (including the Burgers vector **b**, the line direction **u**, the central-beam direction **B**, the foil normal **F** and the thickness t), the program calculates the off-diagonal matrix elements M_{gh} and Stroh's elastic constants for evaluating **R**. These quantities are independent of the variation of the beam direction in an incident cone. In the integration loop, the integration is carried out inside the circle defined by the intersection of the incident cone and the top surface of the specimen. For a point in the circle, s_g is calculated according to the beam direction and the coordinate of the starting point of the integration is determined from the position of the beam cross over and the beam direction. The finishing point of the integration is just t' below the starting point along the direction of the central incident beam, which is the axis of the incident cone. After an integration is completed and the intensity for one point is obtained, the same procedure is repeated with different beam direction and starting value for the next point until the integration has scanned across the circle. When the integration loop is completed the intensity distribution is displayed as a half-tone pattern (Head *et*

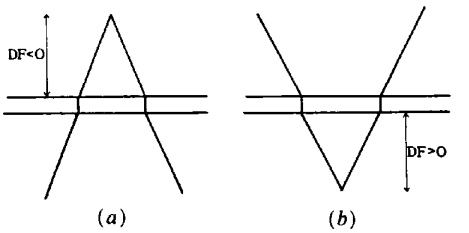

Fig. 1. Ray diagram in the case of convergent-beam electron diffraction. The beam cross over is (*a*) above the specimen (DF < 0) and (*b*) below the specimen (DF > 0).

al., 1973). For the sake of comparison among patterns, the calculation and the display are so arranged that the line direction of the dislocation is always pointing vertically down and the line scanning direction is always horizontal.

The program is executed on an IBM-PC personal computer with an 8087 co-processor. For a typical Tanaka pattern, about 700 points from a silicon specimen 100 nm thick containing a dislocation, the calculating time is about 2 h. The computing time can be reduced by consideration of the symmetry. For example, for an edge dislocation with its projection across the middle of the pattern, the computing time can be reduced by a factor of four.

3. Computation results

Fig. 3 shows calculated and experimental [001] bright-field CBED patterns from perfect Si. Five beams are included in the calculated pattern, they are 000, ±220 and ±$\bar{2}$20. On the whole, the experimental pattern (Fig. 3*a*) and the calculated one (Fig. 3*b*) agree well; both have the zeroth-order fringes forming squares. There are some differences in detail around the edge of the pattern, especially at the corners of the largest square. This discrepancy between the experimental and calculated patterns may mainly be because there are many reflections being excited to some extent at zone-axis incidence during an experiment, but only five beams are considered in the calculation. In the central area of the calculated pattern, where the agreement is good, the intensity distribution is mainly due to the interaction among the five beams included. In this work, we are only interested in the central part of the pattern and its distortion, thus five beams are a sufficiently good approximation for this purpose.

The experimental and calculated patterns from a positive edge dislocation (*i.e.* the extra half plane of an atom is above the dislocation line) in Si are shown in Figs. 4(*a*) and (*b*) and those from a negative edge in Figs. 4(*c*) and (*d*). In all patterns in Fig. 4, the beam cross over is above the specimen. The Tanaka patterns from the edge dislocations in Fig. 4 are no longer square, but are compressed (Figs. 4*a* and *b*) or elongated (Figs. 4*c* and *d*) along a direction perpendicular to the shadow image, depending upon the sign of the Burgers vector. The shadow images of the dislocations in Fig. 4 are shown vertically, which seems to have stronger contrast in the calculated patterns than in the experimental one. The shadow images in the calculated pattern are less reliable since at the vicinity of the dislocation the integration column is shifted sideways to avoid the severely distorted area near the dislocation core.

In Fig. 4 the beam cross over is above the specimen for both calculated and experimental patterns. However, according to Wen *et al.* (1989), when the position of the beam cross over is below the specimen,

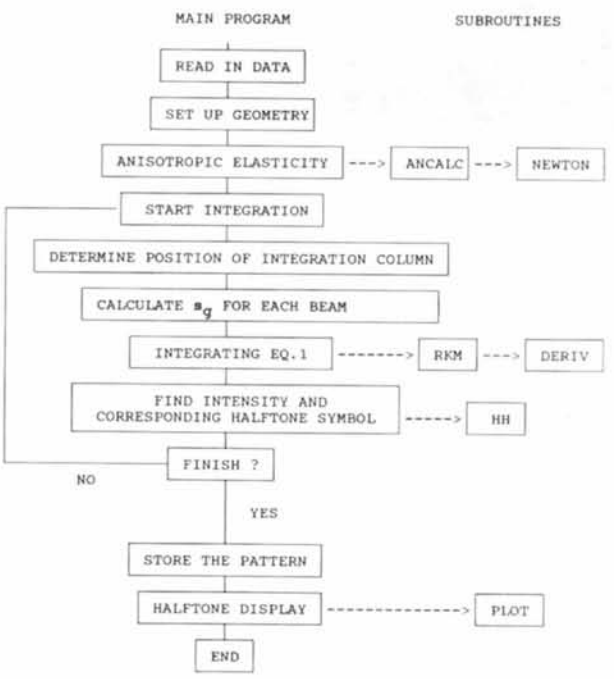

Fig. 2. Flow chart of the program.

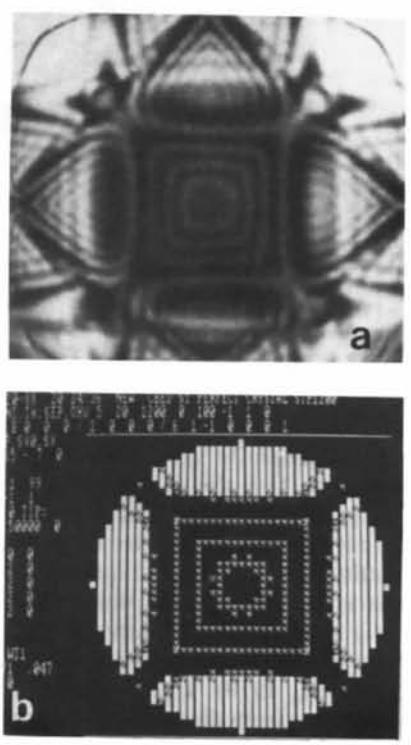

Fig. 3. (*a*) Experimental and (*b*) five-beam calculated CBED patterns from an Si perfect specimen. The thickness is 100 nm.

distortion of the ZOLZ pattern reverses. The calculated CBED patterns in Fig. 5 support this point.

We now consider some simple cases in a f.c.c. crystal where dislocations are of pure edge, pure screw and 60° characters. When looking down along the [001] direction in a cubic system, there are four different configurations for edge dislocations of $\langle 110\rangle/2$-type Burgers vector. For pure screw and 60° dislocations there are two and three distinct cases, respectively. These are listed in Table 1 and are shown

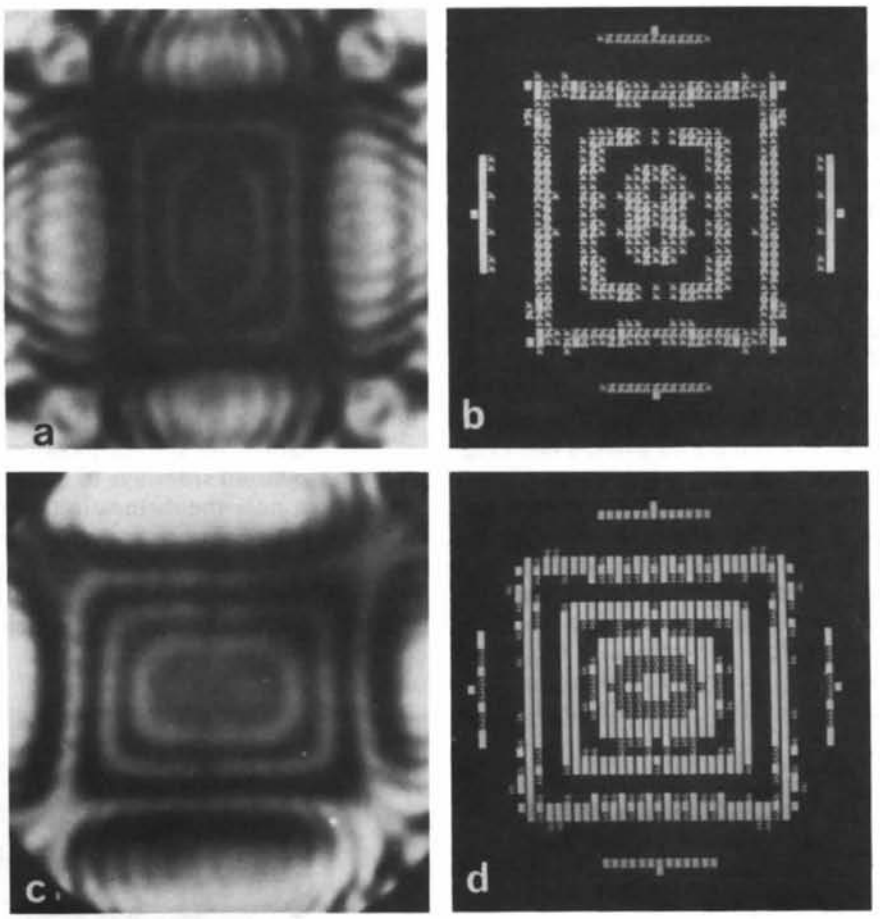

Fig. 4. Tanaka patterns from edge dislocations with the beam cross over above the specimen; (*a*) and (*b*) are experimental and calculated patterns from a positive edge dislocation, (*c*) and (*d*) are those from a negative edge dislocation. Parameters in the calculated patterns are (*b*) $\mathbf{b}=[110]/2$ and (*d*) $\mathbf{b}=[\bar{1}\bar{1}0]/2$; $\mathbf{u}=[1\bar{1}0]$, $t=1000$ Å, DF = 30 μm.

in Fig. 6. Fig. 7 shows computer simulations for all these nine cases, each from a pair of dislocations of opposite Burgers vector. In these calculated patterns, distortions are generally seen. One observes, from these calculations, that the distortion of the patterns from the opposite Burgers vector is of a different sense and that the distortions are of pure compression/elongation, pure shift of the two halves of the pattern separated by the shadow image of the dislocation line or a combination of these two.

In Si, most of the dislocations are dissociated (*e.g.* Ray & Cockayne, 1970). Fig. 8 shows a series of calculated patterns from dissociated dislocations with different separations in an Si specimen. All other parameters in this calculation are the same as that in Fig. 7(*b*1). Comparison of Figs. 8 and 7(*b*1) indicates that the elongated feature remains until the separation is over 30 nm. This value is much greater than that commonly observed experimentally.

The above calculated Tanaka patterns are computed with the distance between the beam cross over and the specimen, DF, being 30 μm. In this case the beam spot on the specimen is about 0·5 μm for an angle range of about 1°. The influence of this DF value on the distortion of the CBED pattern is seen from Fig. 9 for Si. When DF is reduced to 7 μm, the pattern remains similar provided s_g varies within the same range. However, when DF is down to 3 μm the distortion begins to become irregular. Further reduction of DF makes the pattern hardly recognizable as being elongated perpendicular to the shadow image (Fig. 9*e*), as in the case of a normal CBED pattern

Table 1. *The nine distinct cases of edge, screw and 60° dislocations when looking along the* [001] *axis*

Case	Character	**u**	**b**	Glide plane
1	Edge	[110]	$[\bar{1}10]/2$	Stair rod
2	Edge	[112]	$[\bar{1}10]/2$	$(\bar{1}\bar{1}1)$
3	Edge	$[2\bar{1}1]$	[011]/2	$(\bar{1}\bar{1}1)$
4	Edge	[101]	$[\bar{1}01]/2$	Stair rod
5	Screw	[110]	[110]/2	
6	Screw	[101]	[101]/2	
7	60°	[101]	[110]/2	$(\bar{1}11)$
8	60°	[101]	$[0\bar{1}1]/2$	$(\bar{1}11)$
9	60°	[110]	[011]/2	$(1\bar{1}1)$

from a dislocation. This is consistent with the experimental observations [*e.g.* Fig. 5 of the paper by Carpenter & Spence (1982)]. When DF is negative and large in absolute value, *i.e.* the beam cross over is well above the specimen, the pattern becomes regular and its distortion reverses.

4. Discussion

The above calculations show clearly the relative shift of the two parts of the patterns as experimentally observed. If a comparison is made with the experimental pattern, however, it is of importance to have the sense of the shift correct. In the calculation, precautions have been taken to ensure this. Firstly, we make sure that the order of the scan of integration and the display is consistent. An inconsisistency in these two will make the calculated pattern mirror reflected, probably leading to a false determination of the sense of the shift. Secondly, we ascertain that the input **b**, **u**, which are given in Miller indices, and the dislocation configurations expected are consistent. This is done by carefully following the RH/FS perfect-crystal convention, which is compatible with the displacement of the dislocation as evaluated using Stroh's formulation (Head *et al.*, 1973). The agreement of the computed and experimental patterns in Fig. 4 indicates that the sense of the shift in the calculated pattern is correct.

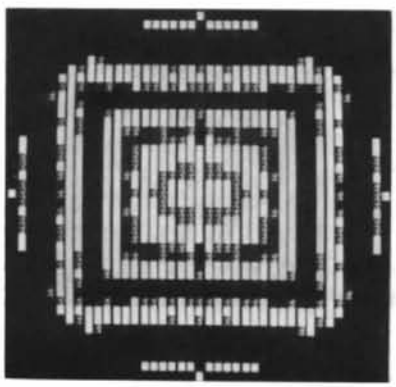

Fig. 5. Calculated pattern from a positive edge dislocation as in Fig. 4(*a*) with the beam cross over below the specimen.

From Fig. 7, the distortion of the ZOLZ pattern from a dislocation can be summarized as follows: (*a*) the pattern can be considered to be divided into two parts separated by the shadow image of the dislocation and the distortion can be considered as a relative shift of these two parts along the Burgers vector; (*b*) the sense of the shift depends on the sign of the Burgers vector and position of the beam cross over relative to the specimen height and (*c*) to determine the sense of the shift of the pattern, one may define a vector $\mathbf{v} = \mathbf{u} \times \mathbf{c}$, where **c** is the vector pointing from the dislocation line to the beam cross over. The side of the pattern to which **v** points moves along the direction of **b**, while the other side of the pattern moves along $-\mathbf{b}$. These properties are in agreement with those derived experimentally (Wen *et al.*, 1989).

With the assumption that dislocations in a f.c.c. lattice have a {111}⟨110⟩ slip system (*e.g.* Hirth & Lothe, 1980), much information about a dislocation can be obtained from a [001] Tanaka pattern alone. When the shadow image of the dislocation is parallel to a ⟨110⟩ direction as in cases 1, 2, 5 and 9 (see Table 1 and Fig. 7), the distortion of the ZOLZ pattern and the corresponding dislocation geometry are listed in Table 2. In this table, columns 1 and 2 are the cases and the dislocation characters as in Table 1, column 3 shows the distortion, column 4 contains **b**′, the projection of **b** on the (001) plane, derived from the distorted pattern in column 3, columns 5 and 6 are the possible **u** and **b**, respectively, according to the distorted pattern. The results in Table 2 are readily verified by looking at Fig. 6. We take the pattern in row 7 of Table 2 as an example. The movement of

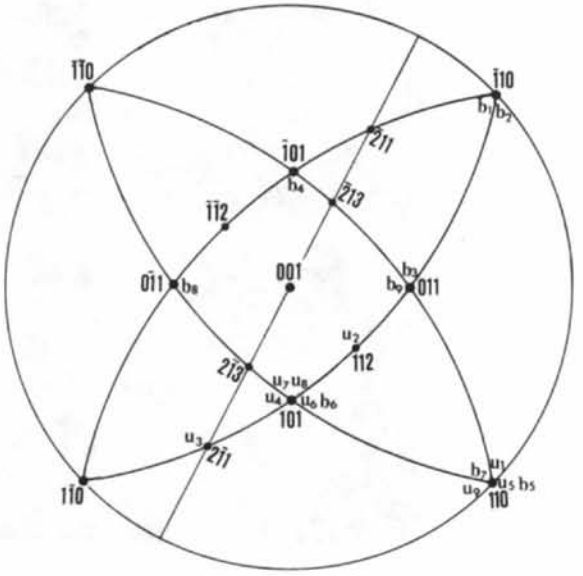

Fig. 6. Stereographic view of the nine distinct cases of edge, screw and 60° dislocations. The straight line indicates the direction which can have projection as the line direction in Fig. 7(*c*) (for details, see text).

the right half of this pattern is towards the bottom right (direction of **b**′ in Table 2), resulting in the pattern being elongated perpendicular to and shifted down along the shadow image of the distortion. Fig. 6 indicates that the ⟨110⟩ direction which can have the appropriate projection direction (**b**′) is either ⟨011⟩ or ⟨01$\bar{1}$⟩, as given in column 6 of Table 2. On the other hand, Table 2 covers all possible cases of dislocations of ⟨110⟩/2 Burgers vector whose lines are parallel to [110]. Note that the distortion of the patterns in rows 1 and 3 and rows 2 and 4 are similar but one can tell which is the case by the length of

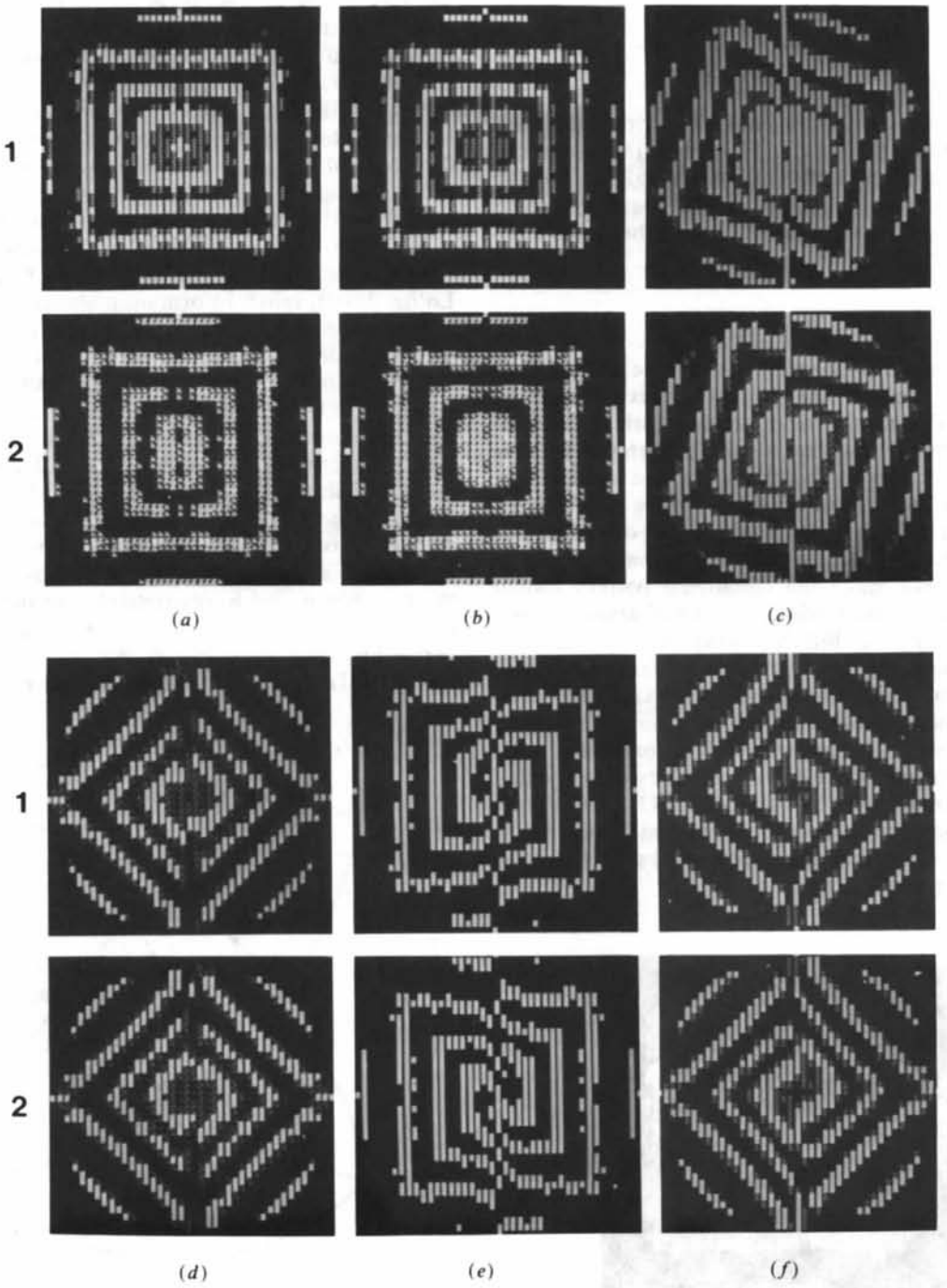

Fig. 7. Calculated Tanaka patterns corresponding to the nine cases in Fig. 6. (*a*) to (*i*) are nine pairs of ±**b** patterns, corresponding to the nine cases in Table 1 and Fig. 6. Rows 1 and 2 are pairs of patterns of opposite Burgers vector. In all the patterns, **u** points down vertically, and the vector **v** points to the right.

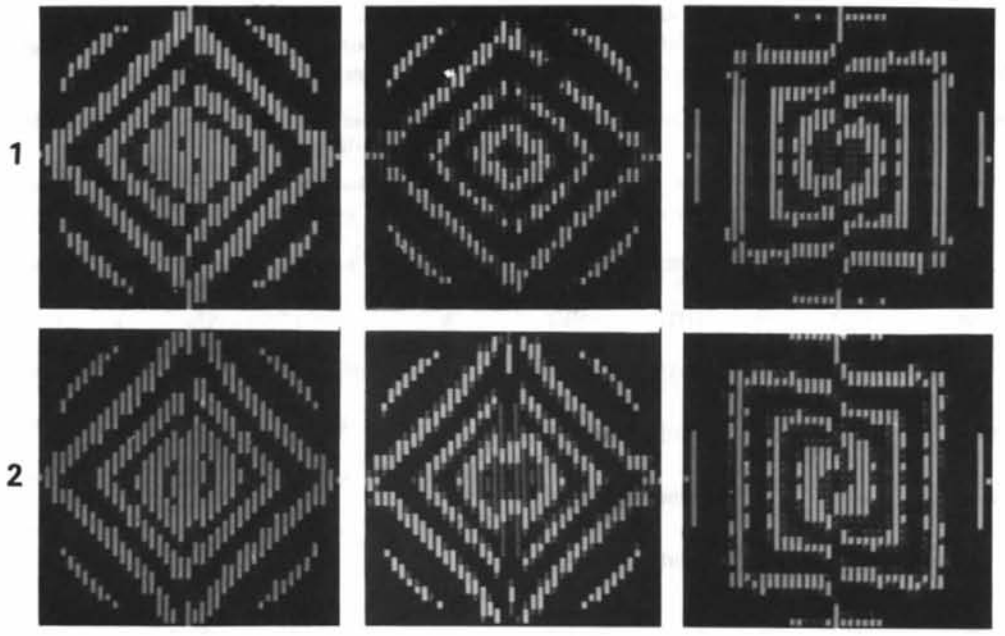

Fig. 7 (*cont.*)

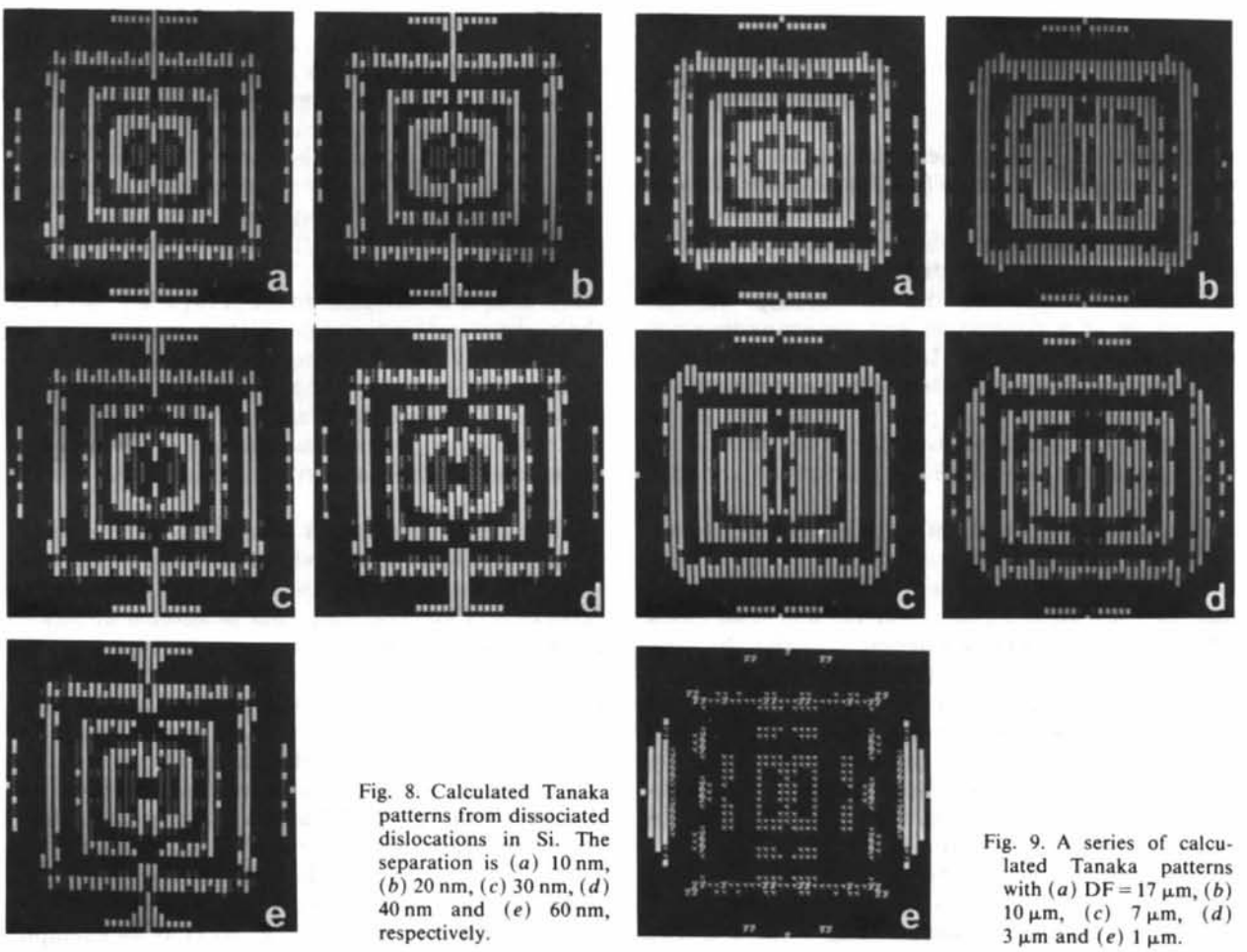

Fig. 8. Calculated Tanaka patterns from dissociated dislocations in Si. The separation is (*a*) 10 nm, (*b*) 20 nm, (*c*) 30 nm, (*d*) 40 nm and (*e*) 60 nm, respectively.

Fig. 9. A series of calculated Tanaka patterns with (*a*) DF = 17 μm, (*b*) 10 μm, (*c*) 7 μm, (*d*) 3 μm and (*e*) 1 μm.

Table 2. *Distortion of Tanaka pattern and geometry of dislocation with projection of* **u** *parallel to the* [110] *direction, which points vertically down*

The beam cross over is below the specimen and the vector $\mathbf{v} = \mathbf{u} \times \mathbf{c}$ points to the right.

Case	Character	Pattern	b′	u	b
1	Edge		→	[110]	$[\bar{1}10]/2$
1	Edge		←	[110]	$[1\bar{1}0]/2$
2	Edge		→	[112]	$[\bar{1}10]/2$
2	Edge		←	[112]	$[1\bar{1}0]/2$
5	Screw		↓	[110]	[110]/2
5	Screw		↑	[110]	$[\bar{1}\bar{1}0]/2$
9	60°		↘	[110]	[011]/2 $[01\bar{1}]/2$
9	60°		↖	[110]	$[0\bar{1}\bar{1}]/2$ $[0\bar{1}1]/2$
9	60°		↙	[110]	[101]/2 $[10\bar{1}]/2$
9	60°		↗	[110]	$[\bar{1}0\bar{1}]/2$ $[\bar{1}01]/2$

Table 3. *Distortion of Tanaka pattern and geometry of dislocation with projection of* **u** *parallel to the* [100] *direction, which points vertically down*

The beam cross over is below the specimen and the vector $\mathbf{v} = \mathbf{u} \times \mathbf{c}$ points to the right.

Case	Character	Pattern	b′	u	b
4	Edge		↑	[101]	$[\bar{1}01]/2$
4	Edge		↓	[101]	$[10\bar{1}]/2$
6	Screw		↓	[101]	[101]/2
6	Screw		↑	[101]	$[\bar{1}0\bar{1}]/2$
7	60°		↘	[101]	[110]/2
7	60°		↖	[101]	$[\bar{1}\bar{1}0]/2$
7	60°		↙	[101]	$[1\bar{1}0]/2$
7	60°		↗	[101]	$[\bar{1}10]/2$
8	60°		←	[101]	$[0\bar{1}1]/2$
8	60°		→	[101]	$[01\bar{1}]/2$

the shadow image since these dislocations in a specimen with surface close to (001) have quite different [001] projections (see Fig. 6).

In the cases where the shadow image of a dislocation is parallel to a ⟨100⟩ direction, *i.e.* to a diagonal of the ZOLZ pattern, the relationship between geometries of a dislocation and corresponding patterns are listed in Table 3. In this table, the distortion of the pattern of the pure edge and pure screw dislocations (cases 4 and 6) is pure shift parallel to the shadow image, while the distortion of 60° dislocations in the table has a component perpendicular to the shadow image.

Although substantial information about dislocations of simple cases can be obtained from a [001] LACBED pattern, it is noticed from Tables 2 and 3 that there are uncertainties for **u** and **b** in some cases. There are two possible **u**'s in case 2 to give the same [001] projection, that is, [112] and $[11\bar{2}]$. Similar ambiguity exists in all cases in Table 2. However, in many investigations, one can choose **u** arbitrarily from the two equivalent crystallographic directions and then **b** is determined accordingly. If a specific determination of **u** is required, it can be done by tilting the specimen about a direction perpendicular to the shadow image. The variation in projection length of the dislocation allows **u** to be determined uniquely. Ambiguity in determining **b** exists in two 60° cases, *i.e.* cases 8 and 9, as well as cases 4 (stair-rod edge) and 6 (screw). This ambiguity occurs because the directions of the Burgers vectors in these cases are mirror images of each other through the (001) plane so that they have the same (001) projections. There are four pairs of these directions of **b** which cannot be determined uniquely. These are [011] and $[01\bar{1}]$, $[0\bar{1}\bar{1}]$ and $[0\bar{1}1]$, [101] and $[10\bar{1}]$ and $[\bar{1}0\bar{1}]$ and $[\bar{1}01]$, as seen from Fig. 6. The directions of **b** which allow unique determination are $[1\bar{1}0]$ and [110] since their mirror images through (001) are themselves. The simplest way to avoid the above uncertainty is to image the dislocation in the two-beam condition (*e.g.* Head *et al.*, 1973) with an appropriate diffraction vector which is perpendicular to one of the two possible Burgers vectors as derived from the [001] Tanaka pattern.

The edge dislocation in case 3 is a representative of general dislocations whose shadow image in a [001] Tanaka pattern is in a direction other than a ⟨110⟩ or a ⟨100⟩. There are four possible **u** directions for such a dislocation, as shown in Fig. 6 as the intersects of the straight line with the four {111} planes. For each of the four line directions there are three possible Burgers vectors, corresponding to the three ⟨110⟩ directions on the same {111} plane. The Burgers vector of the dislocation can be determined uniquely from a [001] Tanaka pattern, or with an extra two-beam image, depending on whether it has a (001) mirror image as discussed above. The determined Burgers vector reduces the possibilities of **u** from four to two. We take Fig. 7(*c*1) as an example.

The possible **u** directions, whose [001] projection is like that shown in Fig. 7(*c*1), are $[2\bar{1}1]$, $[2\bar{1}3]$, $[\bar{2}13]$ or $[\bar{2}11]$ (Fig. 6). The right-hand half of the Tanaka pattern is seen to move up and towards the right, *i.e.* **b**′ points to the two o'clock position. From Fig. 6, this corresponds to $\mathbf{b}=[011]/2$ or $[01\bar{1}]/2$. The line direction **u** is $[2\bar{1}1]$ or $[\bar{2}13]$ for $\mathbf{b}=[011]/2$, and $[2\bar{1}3]$ or $[\bar{2}11]$ for $\mathbf{b}=[01\bar{1}]/2$. To determine **u** uniquely, a tilt about, say, [110] is needed. Calculated patterns in Fig. 10 show the pattern distortion from dislocations with $\mathbf{u}=[2\bar{1}1]$ and $[2\bar{1}3]$, respectively. It shows that these dislocations are indeed distinguishable.

The above discussions are relevant to an Si crystal with the diamond structure. For a simple f.c.c. structure, the distortion of a ⟨001⟩ Tanaka pattern will appear different since the 200-type reflections become the most important ones at a ⟨001⟩ zone axis. In this case, one will expect the shift along a side of the square pattern in Si to become a shift along a diagonal of the pattern in a f.c.c. structure. On the other hand, in a crystal of sphalerite structure, the pattern and its distortion become complicated owing to the residual 200 forbidden reflections. The feasibility of applying the distortion of ZOLZ patterns to study dislocation geometry in these crystals is under investigation.

Compared with other methods of studying dislocation geometry, the unique feature of this LACBED method is that it provides directly the orientation of the projection of **u** and the sign of the Burgers vector in a distorted pattern, and this seems to be independent of the conditions $\mathbf{g}\cdot\mathbf{b}=0$ and $\mathbf{g}\cdot\mathbf{b}\times\mathbf{u}=0$. This allows a quick determination of the geometric properties of a dislocation and the method is less influenced by the elastic anisotropy of the material. The disadvantages of this method are that the distortion in the ZOLZ pattern is best observed on the ⟨001⟩ axis, while it is not so profound in other orientations, and the distortion may not be clearly seen in some materials where it is not possible to have a square pattern even on the ⟨001⟩ zone axis in a perfect area. These limit the usefulness of this method.

5. Summary

(*a*) The observed regularly distorted ZOLZ pattern in a [001] bright-field Tanaka pattern from pure edge, pure screw and 60° dislocations are simulated with the column approximation and the anisotropic elasticity of dislocation. The agreement of the calculated and experimental patterns is good.

(*b*) The distortion in the pattern can be treated as a relative shift of the two halves of the pattern separated by the dislocation. The shift of the half pattern to which the vector $\mathbf{v}=\mathbf{u}\times\mathbf{c}$ points is parallel to the projection of the Burgers vector on the (001) plane.

(*c*) The defocus value of the Tanaka pattern is an important factor in the calculation. When it is small the calculated pattern is irregularly distorted. This is consistent with the experiment.

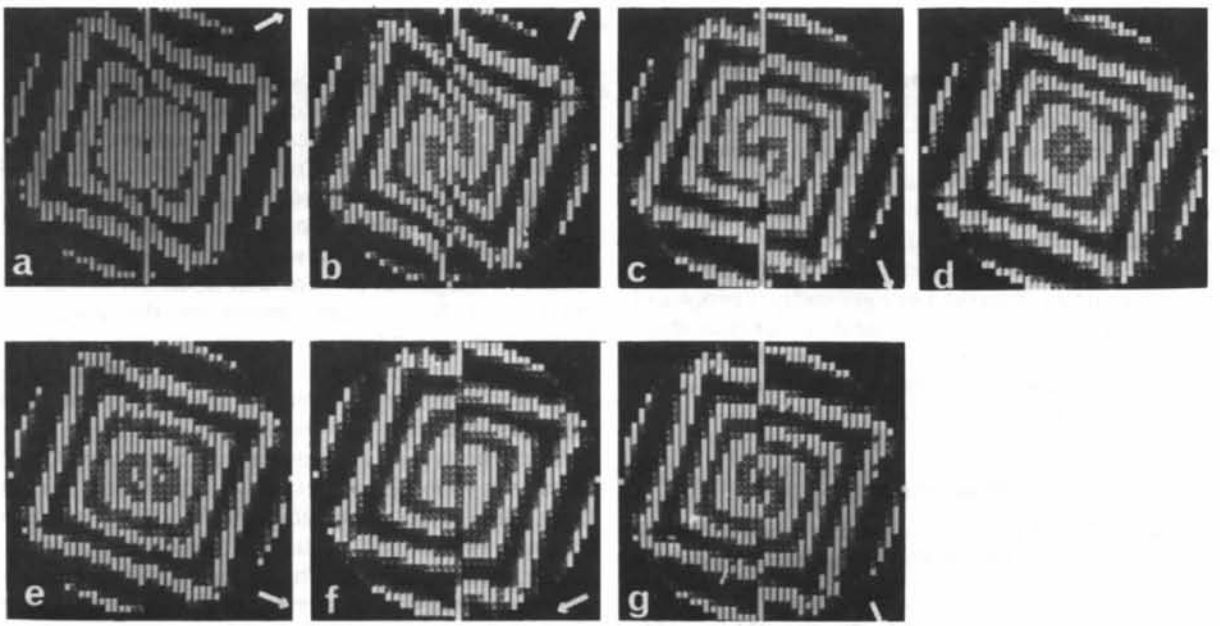

Fig. 10. Calculated patterns with the projection of **u** as in Fig. 7(*c*). **u** is $[2\bar{1}1]$ for (*a*) to (*c*), and $[2\bar{1}3]$ for (*e*) to (*g*). The Burgers vectors are (*a*) [011]/2, (*b*) $[\bar{1}10]/2$, (*c*) [101]/2, (*e*) [110]/2, (*f*) $[0\bar{1}1]/2$ and (*g*) [101]/2. Note that the patterns in (*c*) and (*g*) are very similar because they have the same Burgers vector. The pattern in (*d*) is from a perfect area for comparison.

(*d*) The calculation shows that substantial information about dislocation geometry can be obtained from a distorted [001] Tanaka pattern. In some cases this allows the dislocation to be identified uniquely. In general a unique determination of geometric properties needs an extra two-beam image.

(*e*) The advantage of this method is that the projection of **u** and **b** can be directly observed during TEM observation. This is good for *in situ* investigation. Its disadvantages are that it requires observations at a special orientation (a ⟨001⟩ axis) and that it may not be applied to materials where there is no square-like ZOLZ pattern in a perfect area.

The authors are grateful to Professor Z. Zhou of Beijing Science and Technology for helpful discussions. Mr X. G. Zhang and Mrs K. P. Xu of the Institute of Anshan Iron and Steal Research and Mrs A. X. Li of Shenyang Institute of Metal Research are thanked for assistance in deforming crystals. GL thanks the National Postdoctorial Committee of China for the postdoctoral fellowship.

References

BIAN, W. M. (1986). *J. Chin. Electron Microsc. Soc.* **5**, No. 3, 46. (In Chinese.)

CARPENTER, R. W. & SPENCE, J. C. H. (1982). *Acta Cryst.* A**38**, 55-61.

CHERNS, D., KIELY, C. J. & PRESTON, A. R. (1988). *Ultramicroscopy*, **24**, 355-369.

CHERNS, D. & PRESTON, A. R. (1986). Proc. XIth Int. Congr. on Electron Microscopy, Kyoto, Japan, pp. 721-722.

COWLEY, J. M. (1981). *Diffraction Physics*, p. 196. Amsterdam: North-Holland.

HEAD, A. K., HUMBLE, P., CLAREBROUGH, L. M., MORTON, A. J. & FORWOOD, C. T. (1973). *Computed Electron Micrographs and Defect Identification.* Amsterdam: North-Holland.

HIRSCH, P. B., HOWIE, A., NICHOLSON, R. B., PASHLEY, D. W. & WHELAN, M. J. (1977). *Electron Microscopy of Thin Crystals*, Ch. 9. New York: Robert E. Krieger.

HIRTH, J. P. & LOTHE, J. (1980). *Theory of Dislocations*, 2nd ed., p. 282. New York: John Wiley.

RAY, I. L. F. & COCKAYNE, D. J. H. (1970). *Philos. Mag.* **22**, 853-856.

STROH, A. N. (1958). *Philos. Mag.* **3**, 625-646.

TANAKA, M., SAITO, R., UENO, K. & HARADA, Y. (1980). *J. Electron Microsc.* **29**, 408-412.

TANAKA, M., TERAUCHI, M. & KANEYAMA, T. (1988). *Convergent-Beam Electron Diffraction* II. Tokyo: JEOL-Maruzen.

WEN, J., WANG, R. & LU, G. (1989). *Acta Cryst.* A**45**, 422-427.

Acta Cryst. (1990). A**46**, 112-123

Extinction in Finite Perfect Crystals: Case of a Sphere

BY M. AL HADDAD* AND P. BECKER†

Laboratoire de Cristallographie, associé à l'Université J. Fourier, CNRS, 166*X*, 38042 *Grenoble CEDEX, France*

(*Received* 6 *December* 1988; *accepted* 7 *September* 1989)

Abstract

The extinction factor in finite perfect crystals is calculated from pure dynamical theory. In particular, a detailed solution is proposed for a sphere, in which case the extinction factor depends on the Bragg angle θ and the parameter (R/Λ), where R is the radius of the crystal and Λ the extinction length. An approximate solution based on the Laue geometry is proposed and corrections to take care of the complex boundary conditions are presented. An expression easily usable in refinement programs is proposed that fits the exact value to better than 1%.

Introduction

Two main difficulties are encountered when developing a model for extinction. The major one is to decide on a coupling scheme between coherent and incoherent contributions to the diffracted intensity. A model based on purely incoherent intensities has been developed by Becker & Coppens (1974, 1975), which essentially corresponds to the assumption of pure 'secondary extinction'. To go beyond this approach, Kato (1980) developed a statistical dynamical theory for the propagation of X-rays or neutrons in a distorted crystal. In this new approach, the separation between coherent and incoherent components of the intensity is rather subtle, which shows that 'secondary' and 'primary' extinction are not independent concepts and that the celebrated mosaic model is invalid. The present authors have reformulated Kato's ideas in a more general way (Al Haddad & Becker, 1988; Becker & Al Haddad, 1989, 1990; see also Guigay, 1989). This statistical theory contains the purely incoherent coupling as one limiting case. At the other limit, one also retrieves the purely coherent or dynamical theory that corresponds to 'primary extinction by a perfect crystal'.

The second difficulty has to do with the geometrical boundaries imposed by the sample under study. All

* Present address: Atomic Energy Commission, PO Box 6091, Damascus, Syria.

† Present address: Laboratoire de Minéralogie-Cristallographie, Université Pierre et Marie Curie, Tour 16, 4 Place Jussieu, 75252 Paris CEDEX 05, France.

0108-7673/90/020112-12$03.00